Automatic Generation of Region of Interest for Kidney Ultrasound Images Using Texture Analysis

Wan M. Hafizah, Eko Supriyanto

Abstract— Kidney ultrasound imaging can be used to estimate kidney size and position, and help to diagnose structural abnormalities as well as the presence of cysts and stones. However, due to the presence of speckle noise in ultrasound images, performing the segmentation methods for the kidney images were very challenging and therefore, deleting and removing the complicated background will speeds up and increases the accuracy of the segmentation process. However, in previous studies, the ROI of the kidney is manually cropped. Therefore, this study proposed an automatic region of interest (ROI) generation for kidney ultrasound images. Firstly, some techniques of speckle noise reduction were implemented consist of median filter, Wiener filter and Gaussian low-pass filter. Then texture analysis was performed by calculating the local entropy of the image, continued with the threshold selection, morphological operations, object windowing, determination of seed point and last but not least the ROI generation. This method was performed to several kidney ultrasound images with different speckle noise reduction techniques and different threshold value selection. Based on the result, it shows that for median filter, threshold value of 0.6 gave the highest TRUE ROIs which were 70%. For Wiener filter, threshold value of 0.8 gave highest TRUE ROIs which were 80% and for Gaussian low-pass filter, threshold value of 0.7 gave highest TRUE ROIs which were 100%. By using the previous result, this method has been tested also to more than 200 kidney ultrasound images. As the result, for longitudinal kidney images, out of 120 images, 109 images generate true ROI (91%) and another 11 images generate false ROI (9%). For transverse kidney images, out of 100 images, 89 images generate true ROI (89%) and 11 images generate false ROI (11%). To conclude, the method in this study can be practically used for automatic generation of US kidney ROI.

Keywords—kidney, region of interest, speckle noise reduction, texture filters, ultrasound

I. INTRODUCTION

THE kidneys are retroperitoneal organs, attached to the posterior abdominal wall, covered with the peritoneum and protected by the lower ribs where the kidney can be found just below the liver on the right, and just below the spleen on

the left. During the scanning session, if the kidney were scanned in longitudinal view, the kidney will appear as football-shaped, and in transverse view, the kidney will appear as C-shaped.

The normal kidney has a bright area around it, made up of perinephric fat and Gerota's fascia. The kidney periphery part appear grainy gray, consists of renal cortex and pyramids while the central area of the kidney, the renal sinus, will appear bright (echogenic), and consists of renal sinus fat, calyces, as well as renal pelvis.

Since some other organs lie close to the kidney which may give effect to the performance of other image processing methods, finding a region of interest (ROI) for kidney is quite helpful. Besides, this ROI will improve the speed and accuracy of further segmentation process. Furthermore, many existing kidney ultrasound image processing methods, including enhancement and segmentation techniques have been developed based on a manually selected ROI, not on the whole image [1-4].

Some researchers define ROI as the rough contour or initial contour of the interest object, while the other defines ROI as a rectangular region containing both the interest object kidney and some background information. For this study, a rectangular ROI will be automatically generated and any further operation will be conducted only in that rectangular ROI.

For further segmentation purpose, deleting and removing the complicated background not only speeds up the segmentation process, but also increases accuracy. Therefore, this ROI generation method can be used by any other segmentation method as a preprocessing step since it only cuts the background outside the rectangular ROI while keeping the interest object (kidney) and nearby surrounding tissues untouched.

Automatic ROI has been proposed by other researchers but they were not using the kidney ultrasound images. Yap et al. for example has successfully developed an algorithm to automate the manual process of region of interest (ROI) labeling in computer-aided diagnosis (CAD) for breast lesions [5, 6]. There were other researchers who also focusing on automatically detection lesions in breast ultrasound images [7-9].

However, ROI generation of lesion in breast ultrasound

image is not as complicated as in ROI generation of kidney ultrasound image. In breast images, the shape and edge of the lesion can be easily detected thus, the seed point for generating the ROI is more obvious. Besides, the size of the lesion in the breast images is smaller compared to the size of the kidney. For kidney ultrasound image, in order to generate ROI for the whole kidney image for both longitudinal and transverse view, selection of seed point is quite troublesome.

Thus, in this study, we proposed the development of an automatic ROI generation method that facilitates full automation of kidney ultrasound image segmentation. Therefore, we conducted a texture analysis to the kidney images. As the result, the renal sinus, the central area of the kidney appeared brighter compared to the other part of the images, and in the texture analysis, it also appear as the most common region detected in kidney images.
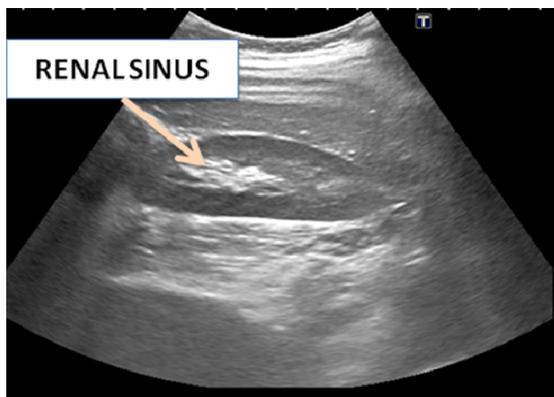

Fig. 1 Ultrasound image of renal sinus of the kidney

So, by using this finding, we have developed an algorithm for automatic ROI generation of ultrasound kidney images consist of speckle noise reduction, texture analysis, threshold selection, morphological operation, objects windowing, seed point determination and lastly ROI generation. The rest of this paper is organized as follows. In section 2, we describe on the materials and the methods applied for generating ROI of the kidney in ultrasound images. The results and analysis are shown in Section 3, and Section 4 shows the conclusion of the study.

II. MATERIALS AND METHODS

For this study, longitudinal and transverse view of ultrasound kidney images were taken from volunteers from Universiti Teknologi Malaysia Johor Bahru (UTM) by using TOSHIBA *AplioMX* ultrasound machine with 3.5MHz transducer. The kidneys were scanned in supine position where the subjects were lying down with the face upward and with inspiration of the subjects. Then, MATLAB programming was used to develop the system for generating the kidney ultrasound region of interest automatically. Fig. 2 shows the longitudinal section of the original ultrasound kidney image while Fig. 3 shows the transverse section of the

image.

Fig. 2 Longitudinal section of original ultrasound kidney image

Fig. 3 Transverse section of original ultrasound kidney image

As explained earlier, the kidney image for longitudinal view is in football-shaped and the image for transverse view is C-shaped. For this study, an automatic defined rectangular ROI will be generated and this ROI generation can be used as a preprocessing step for any other segmentation method since it only cuts the redundant background while keeping the kidney and nearby surrounding tissues untouched. Fig. 4 shows the block diagram of the steps for ROI generation.

Firstly, the speckle noise reductions were performed. For this study, three speckle noise reduction techniques were chosen to be compared consist of median filter, Wiener filter and Gaussian low-pass filter. In order to choose the best filter which helps in optimizing the generation of ROI for kidney US images, comparisons were made between those filters by evaluating their performance in detecting the most ROIs after being tested with several kidney US images. Then texture analysis is implemented for creating texture image and based on the threshold value selected, morphological operation is used for removing unwanted regions. After that, the remaining objects will be windowed so that only one object is chosen as the seed point. Lastly, the ROI is generated according to the seed values.
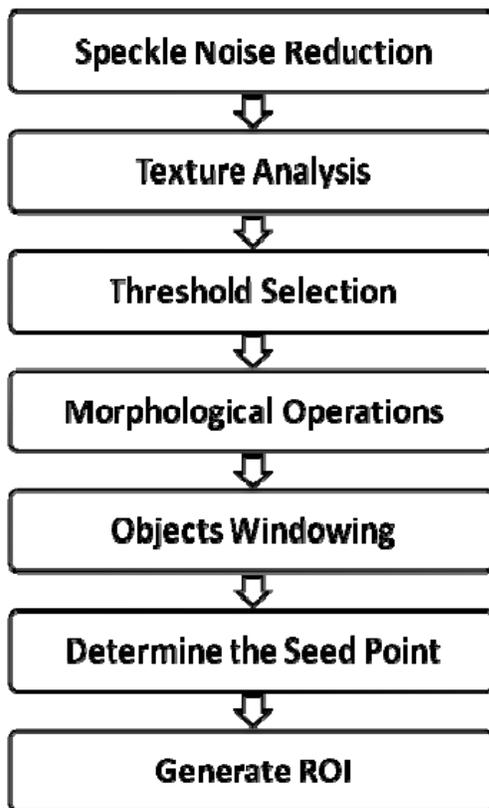
Median filter can help in reducing speckle noise as well as salt and pepper noise [15-17]. The noise-reducing effect of the median filter depends on the neighborhoods' spatial extent and the number of pixels involved in the median calculation.

140	135	124	130	135
128	115	119	123	127
130	124	126	127	140
138	120	150	125	128
125	125	122	135	132

Neighbourhood values: 115, 119, 123, 124, 126, 127, 120, 150, 125

Median Values : 124

Fig. 5 Example for calculating the median value of a pixel neighborhood

Fig. 4 Block diagram for ROI generation

A. Speckle Noise Reduction

Ultrasound image suffers from speckle noise, caused by the interference between coherent waves that is backscattered by the natural surfaces and it is depends on bandwidth, frequency, as well as the position of the transducer [10]. Due to this speckle noise, further image processing such as image segmentation and edge detection has become much more complicated [11, 12]. Therefore, speckle noise reduction techniques can be applied to US image to reduce the noise and improve the image quality by enhancing the contrast of the image [13].

Previously, many researches have been done in this speckle noise reduction area. For example, Yu et al concluded that speckle reducing anisotropic diffusion (SRAD) gives better result on mean preservation, variance reduction, and edge localization compared to the traditional speckle removal filters [12]. Thakur et al, in his research compared various wavelet filters with different thresholding values of US images [14]. Nicolae et al in her research compared three noise reduction techniques, which are median filter, wiener filter and wavelet filters [13, 24-27].

1. Median Filter

Median filter, one of the nonlinear filter types is created by replacing the median of the gray values of pixels into its' original gray level of a pixel in a specific neighborhood. Fig. 5 shows an example to calculate median pixel value.

2. Wiener Filter

Wiener filter inverts the blurring and removes the additive noise simultaneously by performing an optimal tradeoff between inverse filtering and noise smoothing [18]. Besides, Wiener filtering is optimal in terms of the mean square error, where it minimizes the overall mean square error in the process of inverse filtering and noise smoothing. Wiener filtering is also a linear estimation of the original image. The Wiener filter in the frequency domain is as in equation (1):

$$W(f_1, f_2) = \frac{H*(f_1, f_2) S_{xx}(f_1, f_2)}{|H(f_1, f_2)|^2 S_{xx}(f_1, f_2) + S_{\eta\eta}(f_1, f_2)} \quad (1)$$

where $S_{xx}(f_1, f_2), S_{\eta\eta}(f_1, f_2)$ are respectively power spectra of the original image and the additive noise, and $H(f_1, f_2)$ is the blurring filter.

3. Gaussian Low-pass Filter

Gaussian Low-pass filtering has been used in previous researches for removing the speckle noise in US images [19, 20]. Gaussian filter has similar function as median filter but it

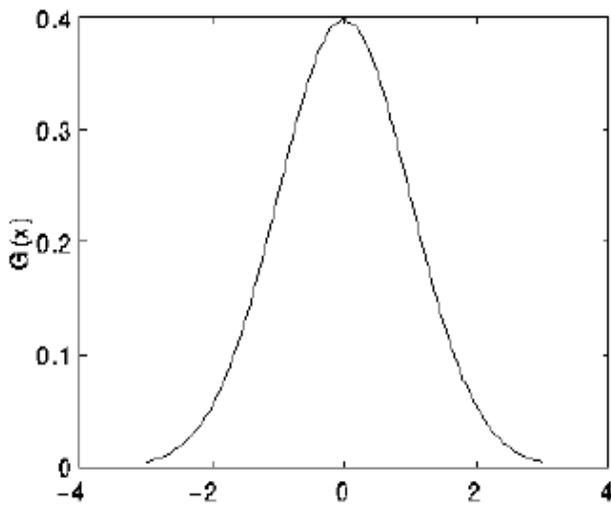uses different kernel, which has the bell-shaped distribution as shown in Fig. 6.

Fig. 6: The bell-shaped of Gaussian distribution

The equation for Gaussian filter is:

$$g(x) = \frac{1}{\sqrt{2\pi}\sigma} e^{\frac{-x^2}{2\sigma^2}} \tag{2}$$

σ in the equation (2) is the standard deviation of the distribution, and also the degree of smoothing. The larger the value of σ, the filtered image is smoother. In order to be accurate, if larger value of σ is used, larger convolution kernel need to be used.

Besides, low-pass filter based on Gaussian function is also common in frequency domain filtering, since both the forward and the inverse Fourier transforms of a Gaussian are the real Gaussian functions [4].

B. Texture Analysis

Texture analysis is important in characterizing regions in an image by their texture content and it is helpful when objects in an image are more characterized by their texture than by intensity, and traditional thresholding techniques cannot be used effectively [26]. When certain values either range, standard deviation or entropy of the image are calculated, they will provide information about the local variability of the intensity values of pixels in the image, thus the texture can be characterized.

The toolbox in MATLAB includes three texture analysis functions that filter an image using standard statistical measures, such as range, standard deviation, and entropy. *rangefilt* is used to calculate the local range of the image. If the image has smooth texture, it will have small value, whereas if the image's texture is rough, the value will be larger. *stdfilt* is used to calculate the local standard deviation of an image while *entropyfilt* is used to calculate the local entropy of a grayscale image which also represents a statistical measure of randomness.

For this study, all three texture filters were applied to the kidney US images. Then, threshold value is set to segment the textures. Threshold value of 0.7 is selected because it is roughly the intensity value of pixels along the boundary between the textures in US kidney images. Depending on the result for texture filtering, only the best filter is chosen to be applied to the rest of kidney US images.

C. Morphological Operations

After image binarization, morphological operations were performed to remove the unwanted regions. Morphological filters are based on two main operations, which are dilation and erosion [21].

The dilation equation is as follows:

$$A \otimes B = \left\{ z | (\hat{B})_z I A \neq \emptyset \right\} \tag{3}$$

where $\emptyset$ is the empty set and $\hat{B}$ is the reflection of the structuring element B. The erosion equation is defined as:

$$A \, \theta B = \left\{ z | (B)_z I A^c \neq \emptyset \right\} \tag{4}$$

where A^c is the complement of A.

In order to extract useful information in images, a small pattern called structuring element is translated over the image [22]. Small objects were removed, and holes were filled using erosion and dilation operations. Spiros et al used morphological closing and opening to segment the nuclei of breast tissue [23].

Since there were possibilities that not all the unwanted regions were removed, the image is windowed again using a center window with 80x80 of height and width, assuming all the kidney images were taken with the kidney is almost at the

center of the image. Only the regions that intersect with this window will be remained as seed point candidates, and the rest will be deleted.

D. Determine the Seed Point

The left regions will undergo another selection steps to determine which is the correct seed point. The algorithm for seed point selection is as in Fig. 7.
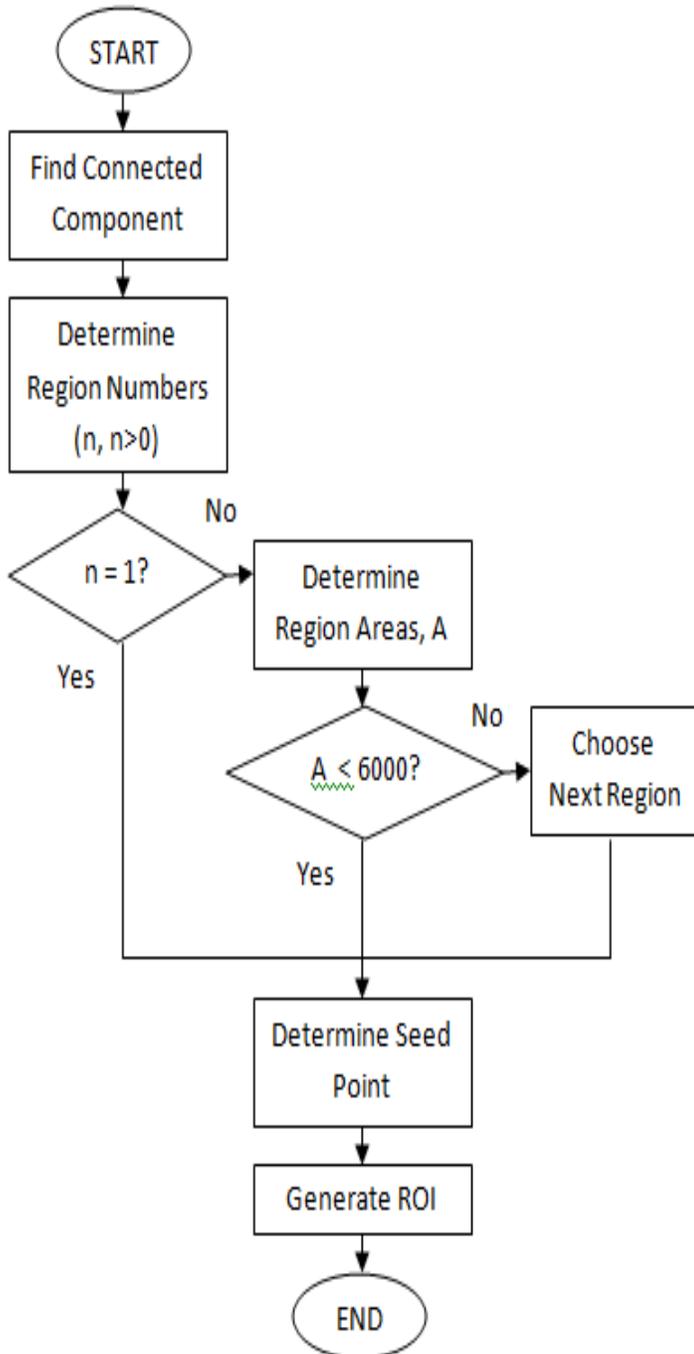
For seed point detection, firstly, the number of connected components (region), n needs to be determined so that we can know how many regions left in the image. If there is only one region left, it is automatically considered as the seed point. If not, the region areas (pixel), A also needs to be determined. We set the threshold pixel areas as 6000. If the area, A is less than 6000, that region is selected as the seed point. If not, the other region will be selected.

Then, the center pixel value (x, y) of the winning region is determined and based on the value, a rectangular window is defined to generate longitudinal and cross section ROI of kidney. For longitudinal kidney image, a window of 400x200 is defined and for transverse kidney image, a window of 240x240 is defined.

The algorithm was tested for more than 200 images and the results were displayed and discussed in the next section.

III. RESULTS AND ANALYSIS

Fig. 8 shows the result of the images after applying speckle noise reduction techniques. Fig. 8(a) is the original image, Fig. 8(b) is the result after median filter, Fig. 8(c) is the result after Wiener filter, and Fig. 8(d) is the result after Gaussian low-pass filter.

Based on the result, the image after median filter and Wiener filter did not differs much but for image after Gaussian low-pass filter, we can see that the image was blurred compared to the original image. All these output images were used for ROI generation to compare which filter gives the best output (number of successful ROIs generated).
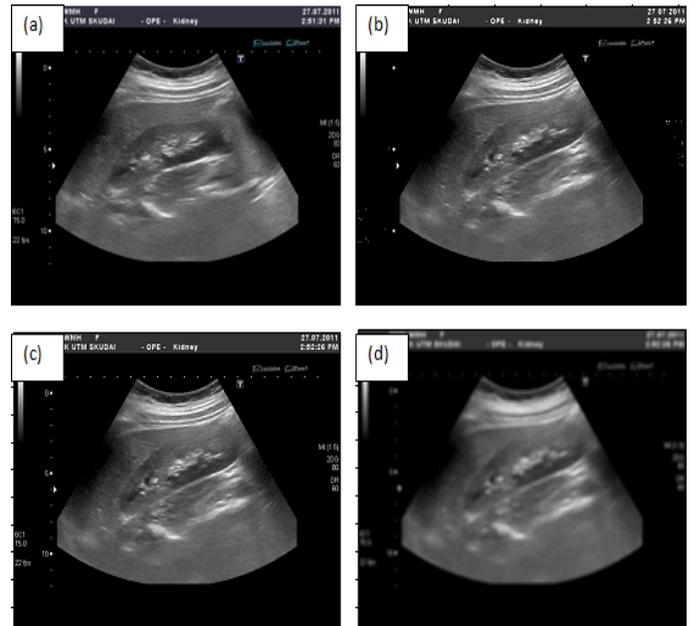

Fig. 8 US kidney image (a) original and after (b) median filter (c) Wiener filter (d) Gaussian low-pass filter

Fig. 7 Algorithm for seed point detection

Then, texture analysis is implemented and the result is changed to binary by setting the threshold value at 0.7. Fig. 9

(a)-(f) show the results of three texture filters which are range filter, standard deviation filter and entropy filter together with their binary images at threshold 0.7.

Based on the result in Fig. 9, it shows that the output for range filter and standard deviation filter detect less texture compared to the output for entropy filter. Besides, after being converted into binary image with the threshold value at 0.7 for all filters, almost nothing were appeared in range filter and standard deviation filter output images. However, for entropy filter output image, there were some regions detected. Therefore, we choose entropy filter to be implemented for the rest of the kidney US images for generating the ROI.
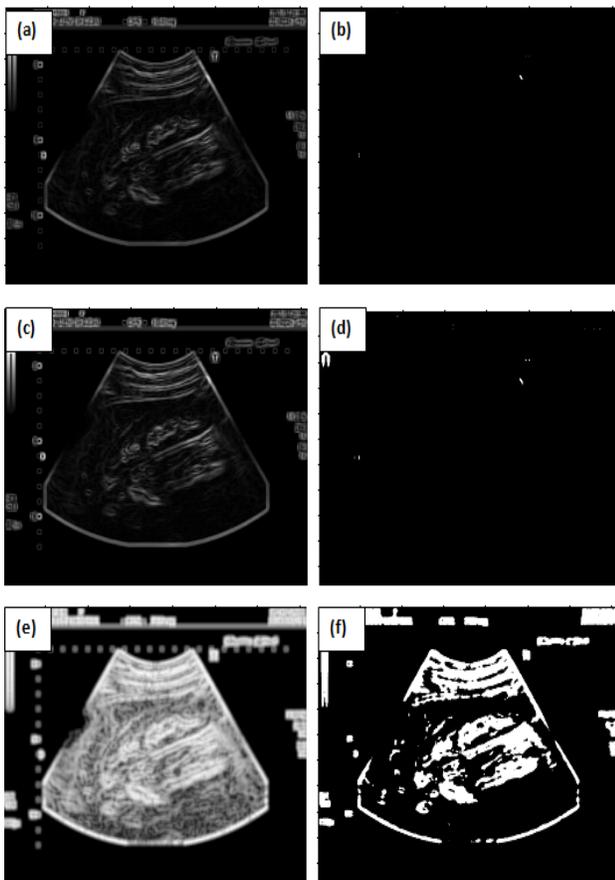

Fig. 9 US kidney image after texture analysis (a) range filter (b) result of (a) with threshold at 0.7 (c) standard deviation filter and (d) result of (c) with threshold at 0.7 (e) entropy filter (f) result of (e) with threshold at 0.7

After that, morphological operation is performed consist of filling the holes and removing small regions by using dilation and erosion theories.There are several operators in MATLAB Image Processing Toolbox such as *bwareaopen, imopen, imclose*, and *imfill. bwareopen* is morphologically open a binary image and remove small object and it is usually used to remove background. *imopen* is function to erodes an image then it will dilate the eroded image using the same SE (structuring element). SE is also known as kernel, which is a small matrix of numbers that is used in image convolutions.

While *imclose* is used to dilate an image and then erodes the dilated image using the same SE. *imfill* is used to fill any holes in the image. For binary image, it changes any connected background pixels to the foreground pixels.

Then, the result is windowed by using a center window with 80x80 height and width, assuming that the kidney is located almost at the centre of the image for both longitudinal and transverse view kidney US images. If the result has more than one region, algorithm as in Fig. 7 will be implemented for selection of a correct seed point. Fig. 10 shows the result for selecting the correct seed point.
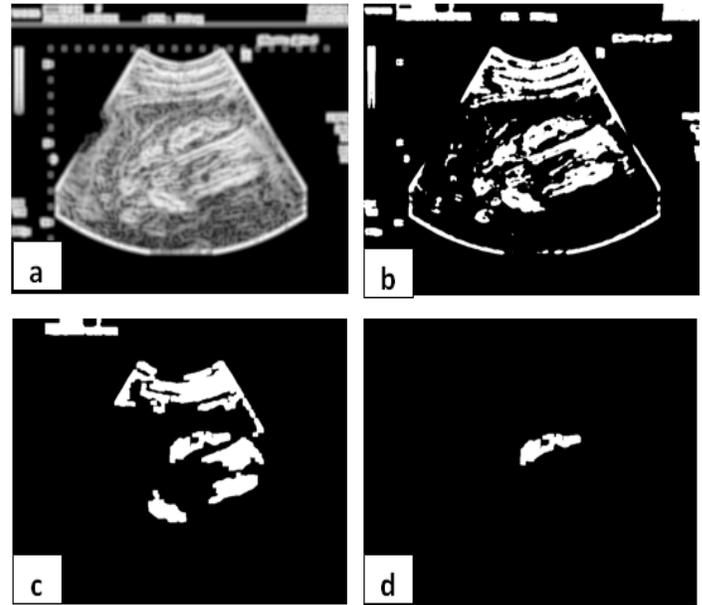

Fig. 10 US kidney image, (a) after texture analysis, (b) binary image with threshold value 0.7, (c) after morphological operations, (d) after windowing.
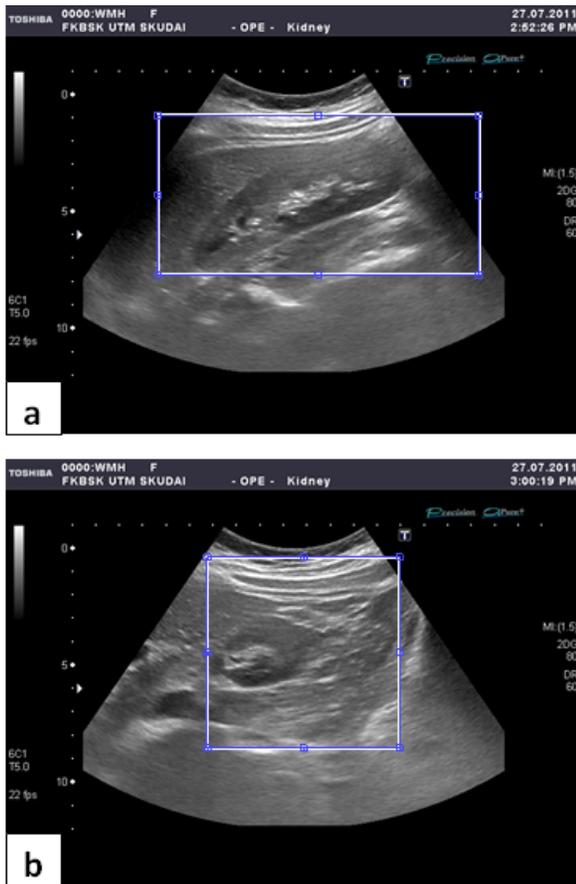
Fig. 11 Automatic ROI generation for (a) longitudinal kidney image, (b) transverse kidney image

After selecting the seed point, the center pixel value of the region is determined. A rectangular window of 400x200 is defined for longitudinal kidney image and 240x240 is defined for transverse kidney image. The result can be seen in Fig. 11 (a) and (b) above.

In order to optimize the result for ROI generation of kidney US images, comparisons have been made by using different types of speckle noise reduction techniques consist of median filter, Wiener filter and Gaussian low-pass filter. For each filter, threshold value is also varied from 0.5 to 0.9 to investigate if the value were affecting the generation of ROIs. Table 1 shows the comparison for generating ROI for different speckle noise reduction techniques.

Table 1 Comparison for generating ROI for different speckle noise reduction techniques

Speckle Noise Reduction Techniques	Threshold Value	ROI	
		TRUE(%)	FALSE(%)
Median Filter	0.5	0	100
	0.6	**70**	**30**
	0.7	40	60
	0.8	40	60
	0.9	0	100
Wiener Filter	0.5	0	100
	0.6	70	30
	0.7	40	60
	0.8	**80**	**20**
	0.9	0	100
Gaussian Low-pass Filter	0.5	90	10
	0.6	30	70
	0.7	**100**	**0**
	0.8	0	100
	0.9	0	100

Based on Table 1, it shows that for median filter and Wiener filter, only threshold value from 0.6 to 0.8 gave TRUE result for ROI generation whereas for Gaussian low-pass filter, threshold value from 0.5 to 0.7 gave TRUE result for ROI generation. For median filter, threshold value of 0.6 gives the highest TRUE ROIs which are 70%. For Wiener filter, threshold value of 0.8 gives the highest TRUE ROIs which are 80% and for Gaussian low-pass filter, threshold value of 0.7 gives the highest TRUE ROIs which are 100%. Therefore, based on the result, we chose Gaussian low-pass filtering for speckle noise reduction technique with the threshold value of 0.7 to be applied to the rest of the images.

The experiment has been done for this study using more than 200 US kidney images for both longitudinal and cross section. For longitudinal kidney images, out of 120 images, 109 images generate true ROI (91%) and another 11 images generate false ROI (9%). For transverse kidney images, out of 100 images, 89 images generate true ROI (89%) and 11 images generate false ROI (11%). The results can be seen in Fig. 12 and Fig. 13.
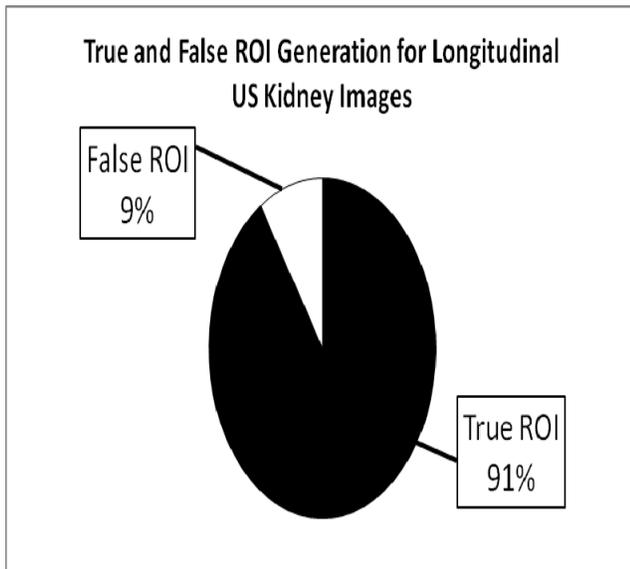
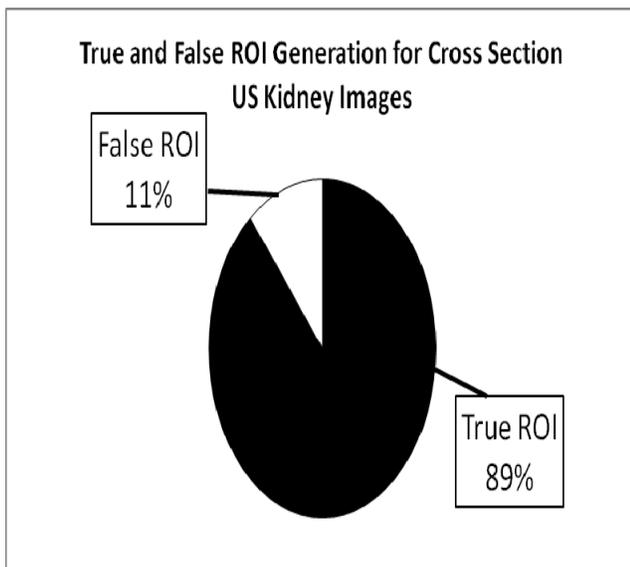Fig. 12 ROI generation for longitudinal US kidney images

Fig. 13 ROI generation for cross section US kidney images.

The false ROI in certain images maybe caused by the noise in kidney US image. Besides, the position of the kidney also plays an important role in generating a true ROI, as in this study, assumption have been made that the kidney is located at the center of the images. That is probably why the algorithm for image processing was failed to generate a true ROI in some images. Nevertheless, about 89% true ROI have been generated for both longitudinal and transverse ultrasound kidney images. Therefore, the method in this study is reliable for automatic generation of US kidney ROI.

IV. CONCLUSION

From the results, it is concluded that for kidney ultrasound images, texture analysis by using entropy filter is better compared to range filter and standard deviation filter. Based on the comparison between speckle noise reduction techniques, Gaussian low-pass filter gave the highest TRUE ROIs which were 100% after being tested using threshold value 0.7. For median filter, threshold value of 0.6 gives the highest TRUE ROIs which are 70% and for Wiener filter, threshold value of 0.8 gives the highest TRUE ROIs which are 80%.

By choosing Gaussian low-pass filtering for speckle noise reduction technique with the threshold value of 0.7 to be applied to the rest of the images, it was proved that this study can be used to automatically detect the seed point of the kidney and successfully generate true kidney ROI until 89%. The generation of true ROI can be used as the preprocessing methods for any other segmentation techniques. This ROI generation can make the next image processing methods is faster as some part of the original image has been cropped.

REFERENCES

[1] Raja, K.B., Reddy, M.R., Swaranamani, S., Suresh, S., Madheswaran, M., Thyagarajah, K., Study on Ultrasound Kidney Images for Implementing Content Based Image Retrieval System using Regional Gray-Level Distribution, *Proc. International Conference on advances in infrastructures for electronic business, education, science, medicine, and mobile technologies on the internet*, L-aquila, Italy, Paper No. 93, Jan 6 – 12, 2003.

[2] Xie, J., Jiang, Y., Tsui, H., Segmentation of Kidney From Ultrasound Images Based on Texture and Shape Priors, *IEEE Trans On Medical Imaging*, Vol. 24, No. 1, 2005.

[3] Raja, K.B., Madheswaran, M., Thyagarajah, K., Quantitative and Qualitative Evaluation of US Kidney Images for Disorder Classification using Multi-Scale Differential Features, *ICGST-BIME Journal*, Volume 7, Issue 1, May, 2007.

[4] Hafizah, W.M., Supriyanto, E., Comparative Evaluation of Ultrasound Kidney Image Enhancement Techniques, *International Journal of Computer Applications,* 2011, Volume 21, No. 7, pp.15-19.

[5] Yap, M.H., Ewe, H.T., Region of interest (ROI) detection in ultrasound breast images. In: *Proceedings of MMU International Symposium on Information and Communications Technologies (M2USIC).* Cyberjaya, Malaysia: Multimedia University; 2005: 5–8.

[6] Yap, M.H., Edirisinghe, E.A., Bez, H.E., A novel algorithm for initial lesion detection in ultrasound breast images, *Journal of Applied Clinical Medical Physics*, Volume 9, Number 4, 2008.

[7] Cheng, H.D., Shan, J., Ju, W., Guo, Y., and Zhang, L., Automated breast cancer detection and classification using ultrasound images: A survey*, Pattern Recognition 43*, 1 (2010), 299-317.

[8] Drukker, K., Giger, M.L., Horsch, K., Kupinski, M.A., Vyborny, C.J., Mendelson, E.B., Computerized lesion detection on breast ultrasound*, Medical Physics 29*, 7 (2002), 1438-1446.

[9] Madabhushi, A. and Metaxas, D.N. Combining low-, high-level and empirical domain knowledge for automated segmentation of ultrasonic breast lesions. *IEEE Trans. on Medical Imaging 22*, 2 (2003), 155-169.

[10] Gupta, S., Chauhan, R. C., Saxena, S. C., Robust non-homomorphic approach for speckle reduction in medical ultrasound images, *Medical and Biological Engineering and Computing*, 2005, 43, 189–195.

[11] Shrimali, V., Anand, R. S., Kumar, V., Comparing the performance of ultrasonic liver image enhancement techniques: a preference study, *IETE Journal of Research*, Vol 56, Issue 1, 2010.

[12] Yu, Y., Acton, S. T., Speckle reducing anistrophic diffusion. *IEEE Trans on Imag Process*, Vol 11, pp 1260-1270, 2002.

[13] Nicolae, M. C., Moraru, L., Onose, L., Comparative approach for speckle reduction in medical ultrasound images, Romanian J. Biophys., Vol. 20, No. 1, P. 13–21, 2010.

[14] Thakur, A., Anand, R. S. Image quality based comparative evaluation of wavelet filters in ultrasound speckle reduction. *Digital Signal Processing* 15, 2005, pp. 455-465.

[15] Arulmozhi, K., Perumal, S. A., Kannan, K., Bharati, S., Contrast improvement of radiographic images in spatial domain by edge preserving filters, *IJCSNS International Journal of Computer Science and Network Security*, 2010, Vol.10 No.2.

[16] Hafizah, M., Tan Kok, Supriyanto, E., 3D Ultrasound Image Reconstruction Based on VTK, *Proceedings of the 9th WSEAS International Conference on SIGNAL PROCESSING*, 2010, pp.102-106.

[17] Hafizah, M., Tan Kok, Supriyanto, E., Development of 3D Image Reconstruction Based on Untracked 2D Fetal Phantom Ultrasound Images using VTK, *WSEAS TRANSACTIONS on SIGNAL PROCESSING*, 2010, Issue 4, Volume 6, pp. 145-154.

[18] A. Khireddine, K. Benmahammed, W. Puech, Digital image restoration by Wiener filter in 2D case, *Advances in Engineering Software* 38 (2007) pp.513–516.

[19] Ramachandrans, S., Nair, M.G., Ultrasound Speckle Reduction Using Nonlinear Gaussian Filters in Laplacian Pyramid Domain. *IEEE 3rd International Congress on Image and Signal Processing (CISP2010).* 2010.

[20] Donka Angelora and Lyudmila Mihaylova. Contour Segmentation in 2D Ultrasound Medical Images with Particle Filtering. *Machine Vision and Application*. 2009.

[21] Maragus, P.A., A representation theory for morphological image and signal processing, *IEEE Transact and Pattern Analys Mach Intellig*, 1989.

[22] Bouaynaya, N., Schonfeld, D., Spatially-variant morphological image processing: theory and applications, in proceedings of *SPIE Visual Communication and Image Process (VCIP'06)*, Vol. 6077, 2006.

[23] Kostopoulos, S., Cavouras, D., Daskalakis A., et al, Assessing Estrogen Receptors' Status by Texture Analysis of Breast Tissue Specimens and Pattern Recognition Methods. *Spinger.* 2007.

[24] Suprianto, E., Hafizah, W.M., Wui, Y.J., Arooj, A., Automatic Non Invasive Kidney Volume Measurement Based On Ultrasound Image, *Proceedings of 15th WSEAS International Conference on Computers*, 2011, pp.387-392.

[25] Suprianto, E., Jamlos, M.A., Kheung, L.K., Segmentation of Carotid Artery Wall towards Early Detection of Alzheimer Disease, *Proceedings of 15th WSEAS International Conference on Computers*, 2011, pp.201-206.

[26] Suprianto, E., Tahir, N.A., Nooh, S.M., Automatic Ultrasound Kidney's Centroid Detection System, *Proceedings of 15th WSEAS International Conference on Computers*, 2011, pp.160-165.

[27] Suprianto, E., Hafizah, W.M., Wong, W.Y., Ultrasound Pancreas Segmentation: A New Approach Towards Detection of Diabetes Mellitus, *Proceedings of 15th WSEAS International Conference on Computers*, 2011, pp.184-188